Langmuir

Article

pubs.acs.org/Langmuir

On the Stability and Morphology of Complex Coacervate Core Micelles: From Spherical to Wormlike Micelles

Hanne M. van der Kooij,*[,†] Evan Spruijt,[†] Ilja K. Voets,[‡] Remco Fokkink,[†] Martien A. Cohen Stuart,[†] and Jasper van der Gucht*[,†]

[†]Laboratory of Physical Chemistry and Colloid Science, Wageningen University, Dreijenplein 6, 6703 HB Wageningen, The Netherlands

[‡]Institute for Complex Molecular Systems and Laboratory of Macromolecular and Organic Chemistry, Eindhoven University of Technology, P.O. Box 513, 5600 MB Eindhoven, The Netherlands

Supporting Information

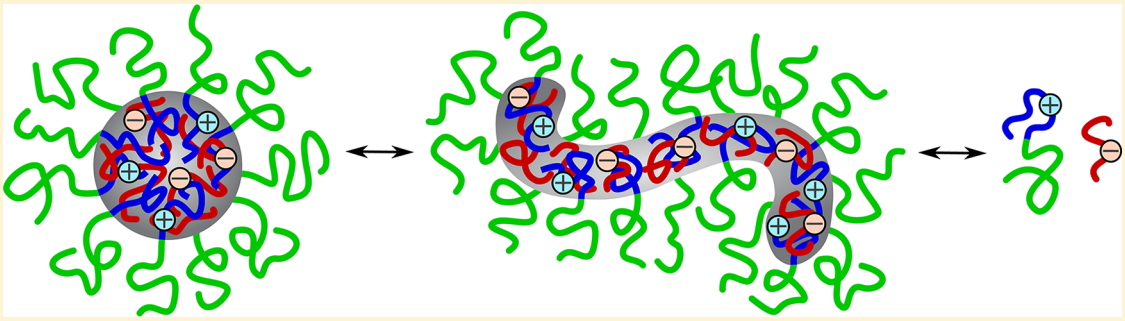

ABSTRACT: We present a systematic study of the stability and morphology of complex coacervate core micelles (C3Ms) formed from poly(acrylic acid) (PAA) and poly(*N*-methyl-2-vinylpyridinium)-*b*-poly(ethylene oxide) (PM2VP-*b*-PEO). We use polarized and depolarized dynamic and static light scattering, combined with small-angle X-ray scattering, to investigate how the polymer chain length and salt concentration affect the stability, size, and shape of these micelles. We show that C3Ms are formed in aqueous solution below a critical salt concentration, which increases considerably with increasing PAA and PM2VP length and levels off for long chains. This trend is in good agreement with a mean-field model of polyelectrolyte complexation based on the Voorn−Overbeek theory. In addition, we find that salt induces morphological changes in C3Ms when the PAA homopolymer is sufficiently short: from spherical micelles with a diameter of several tens of nanometers at low salt concentration to wormlike micelles with a contour length of several hundreds of nanometers just before the critical salt concentration. By contrast, C3Ms of long PAA homopolymers remain spherical upon addition of salt and shrink slightly. A critical review of existing literature on other C3Ms reveals that the transition from spherical to wormlike micelles is probably a general phenomenon, which can be rationalized in terms of a classical packing parameter for amphiphiles.

INTRODUCTION

Complex coacervate core micelles (C3Ms) are polymeric nanostructures with a complex coacervate core and a neutral hydrophilic corona. They coassemble spontaneously from ionic-neutral copolymers and oppositely charged macroions below a critical salt concentration in aqueous solution[1] (Figure 1a). C3Ms are promising candidates for a variety of applications. In solution, they are potential carriers of charged compounds, such as enzymes,[2] DNA,[3] RNA,[4] antibodies,[5] nanoparticles,[6] dendritic photosensitizers,[7] and metal ions,[8] and they can be used to purify wastewater by flocculating charged contaminants.[9] At surfaces, C3Ms act as antifouling agents.[10,11] For these purposes, a knowledge of the stability and morphology of these micelles is essential. When the effects of salt concentration, polymer chain length, and polymer concentration on the stability and morphology of C3Ms are known in detail, these structures can be optimized to meet the desired conditions.

Despite the considerable interest in C3Ms, systematic studies on their stability and morphology are scarce. A majority of studies on the stability of C3Ms deal with the effect of salt. Kabanov et al. were pioneers in this area: they measured a decrease in light-scattering intensity with increasing salt concentration, which they attributed to the disintegration of C3Ms.[12] Later, it was found that both the number and mass of C3Ms are reduced upon addition of salt.[13,14] The decrease in the number of C3Ms is a direct consequence of an increase in the critical micelle concentration (cmc). Beyond a certain critical salt concentration, which varies significantly between

Received: August 8, 2012
Revised: September 13, 2012
Published: September 14, 2012

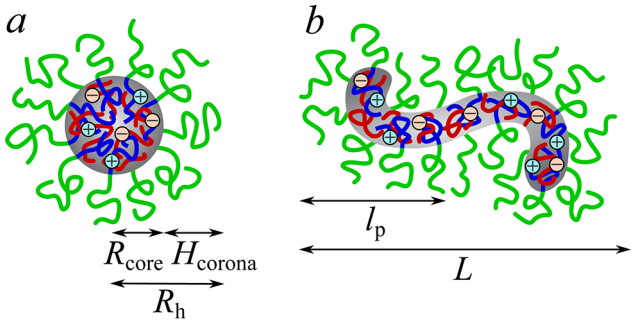

Figure 1. Artist's impression of (a) a spherical and (b) a wormlike complex coacervate core micelle (C3M) formed from cationic−neutral diblock copolymers and anionic homopolymers. The homopolymer chains and cationic blocks constitute the core, whereas the neutral blocks reside in the corona. R_{core} and R_h are the core radius and hydrodynamic radius, respectively. $H_{corona} \approx R_h - R_{core}$ is the corona thickness. l_p and L are the persistence length and contour length, respectively, of the wormlike micelle.

different types of C3Ms,[6] the cmc exceeds the total polymer concentration and all micelles are dissociated. By using the dependence of the critical salt concentration on the polymer concentration, Yan et al. and Wang et al. found that the cmc of C3Ms increases exponentially with the square root of the salt concentration.[13,14] The critical salt concentration also depends on the polymer chain length. This chain length dependence has been studied only qualitatively by Gaucher et al., who concluded that the resistance of C3Ms against salt-induced disintegration (salt stability) improves with increasing homopolymer chain length.[15] Unfortunately, they limited their research to three homopolymer lengths.

Experimental studies on the morphology of C3Ms mainly address the effect of salt on the hydrodynamic radius (R_h). Both an increase[2,13,14,16−24] and a decrease[2,25−27] in R_h upon addition of salt have been reported, but the mechanisms underlying these opposite trends are poorly understood. Yan et al. were the first to show that salt sometimes causes a morphological change in C3Ms.[13] Using cryogenic transmission electron microscopy, they revealed the existence of large aggregates at high salt concentration, of which some seemed to be wormlike micelles. They also observed a peak in light-scattering intensity just before the critical salt concentration. This peak appeared to coincide with a maximum in R_h and a local minimum in the polydispersity index. A similar scattering peak has been reported more often, but generally without explanation.[15,20−22,28] Finally, experiments on the effect of the homopolymer chain length on the morphology of C3Ms are lacking.

In this article, we address these two open questions: how does the polymer chain length affect the salt stability of C3Ms, and why do some C3Ms grow whereas others shrink upon addition of salt? We use light-scattering salt titrations to answer the first question and a combination of various light-scattering techniques and small-angle X-ray scattering to answer the latter. As a model system, we choose micelles formed from anionic homopolymer poly(acrylic acid) (PAA) and cationic−neutral diblock copolymer poly(*N*-methyl-2-vinylpyridinium)-*b*-poly(ethylene oxide) (PM2VP-*b*-PEO) because they are well characterized.[11,29,30] Our measurements indicate that the salt stability of C3Ms improves with increasing chain length for short polymer chains and levels off for longer chains. We support these findings with a model for polyelectrolyte complexation based on the mean-field theory of Overbeek and Voorn.[31] Furthermore, we find that short homopolymers give rise to an increase in the average size of C3Ms upon addition of salt, whereas long homopolymers give rise to a shrinkage of C3Ms. The increase in size is always accompanied by a peak in scattering intensity. We argue that this apparent growth and the increase in intensity are due to a morphological transition from spherical to wormlike micelles, which grow larger with increasing polymer concentration.

The insights we present here allow for the fine tuning of the stability and morphology of these typical coassembled nanostructures. We believe that the underlying principles are more general and also apply to other charge-driven complexes, such as triblock copolymer hydrogels with complex coacervate junction points[32] and complex coacervate membranes.[33]

EXPERIMENTAL DETAILS

Materials. Complex coacervate core micelles (C3Ms) were prepared in aqueous solution from poly(acrylic acid) (PAA), an anionic polyelectrolyte with pH-dependent charges, and poly(*N*-methyl-2-vinylpyridinium)-*b*-poly(ethylene oxide) (PM2VP-*b*-PEO), a cationic−neutral diblock copolymer with pH-independent charges. Polymers with various chain and block lengths were used, as specified in Table 1. $P2VP_{41}$-*b*-PEO_{204} and $P2VP_{128}$-*b*-PEO_{477} were quaternized with iodomethane (99%, Sigma-Aldrich) according to a procedure described elsewhere, leading to a final degree of quaternization (DQ) of approximately 89%.[11] Solid NaCl was purchased from Sigma-Aldrich. Solutions of KOH and HCl (0.10 M each) were obtained from Merck Chemicals. Milli-Q water with a resistivity of >18.2 MΩ was used for all solutions.

Table 1. Specifications of the PAA and PM2VP-*b*-PEO Polymers Used in This Study[a]

polymer	supplier	M_n (kg/mol)	M_w/M_n
PAA_{13}	Polysciences	1.2[b]	1.60
PAA_{20}	Sigma-Aldrich	1.5[c]	1.32[c]
PAA_{47}	Polymer Source	3.4	1.30
PAA_{139}	Polymer Source	10.0	1.15
PAA_{162}	Polymer Source	11.7	1.07
PAA_{500}	Polymer Source	36.0	1.10
PAA_{1630}	Polysciences	153.3[b]	1.60
PAA_{1728}	Polymer Source	124.5	1.25
PAA_{4200}[d]	Sigma-Aldrich	$(3.0 \pm 0.8) \times 10^2$	?
PAA_{11600}[d]	Sigma-Aldrich	$(8.3 \pm 2.1) \times 10^2$	?
PAA_{37000}[d]	Sigma-Aldrich	$(2.7 \pm 0.7) \times 10^3$	?
$PM2VP_{41}$-*b*-PEO_{204}[e]	Polymer Source	4.3-*b*-9.0	1.05
$PM2VP_{128}$-*b*-PEO_{477}[e]	Polymer Source	13.5-*b*-21.0	1.10
$PM2VP_{249}$-*b*-PEO_{134}[f]	Polymer Source	56.5-*b*-5.9	1.05

[a] M_n and M_w are the number- and weight-average molecular weights, respectively. [b] Sodium salt. [c] Determined by gel permeation chromatography (GPC) in 10 mM phosphate buffer. [d] These polymers are ∼0.1% cross-linked. Only the viscosity-average molecular weights (M_v) were specified. The M_n values were estimated to be $M_v/1.5$ (±25%). [e] Purchased in unquaternized form as $P2VP_{41}$-*b*-PEO_{204} and $P2VP_{128}$-*b*-PEO_{477}, respectively. DQ ≈ 89%. [f] DQ ≈ 86%.

Sample Preparation. Stock solutions of PAA (5 g/L) and PM2VP-*b*-PEO (10 g/L) were prepared by dissolving the polymers in water containing 10 mM NaCl. They were filtered through 0.20 μm poly(ether sulfone) membrane syringe filters (Advanced Microdevices Pvt. Ltd.). To ensure that possible polymer adsorption to the filter would not affect the concentration in the filtrate, the first 1 mL of the filtrate was discarded. The stock solutions were mixed in a 1:1 ratio of PAA to PM2VP monomers and diluted with a filtered 10 mM NaCl solution to the desired polymer concentration. The experimental

dx.doi.org/10.1021/la303211b | *Langmuir* 2012, 28, 14180−14191

results were found to be independent of the order of mixing of PAA and PM2VP-*b*-PEO. For measurements at elevated salt concentrations, variable amounts of a filtered 1.0 M NaCl solution were then pipetted slowly into the C3M solution. Finally, the pH was adjusted to 7.1 ± 0.2, where both PAA and PM2VP are almost fully charged, resulting in C3Ms with maximum stability and scattering intensity.[11,30] (See Supporting Information for a titration of $PM2VP_{41}$-*b*-PEO_{204} with PAA_{162}.) All experiments were performed at 20.0 ± 0.3 °C at least 18 h after mixing the polymers. C3Ms formed from PAA_m and $PM2VP_n$-*b*-PEO_o will be referred to as $PAA_m/PM2VP_n$-*b*-PEO_o. Polymer concentrations will be expressed as acrylic acid monomer concentrations (c_{AA}) in mM.

Light Scattering. *Titrations.* Light-scattering titrations were performed on an ALV instrument equipped with an ALV5000/60X0 external correlator and a 300 mW Cobolt Samba-300 DPSS laser operating at a wavelength (λ) of 532 nm. The detection angle (θ) was 90°. A Schott−Geräte computer-controlled titration setup was used to regulate the addition of titrant, stirring, and delay time between additions. In salt titrations, the titrant was a 1.0 M NaCl solution at pH 7.1 ± 0.2, filtered through a 0.20 μm poly(ether sulfone) membrane syringe filter (Advanced Microdevices Pvt. Ltd.). Both the stirring and delay time were typically 60 s. After each addition of titrant, the light-scattering intensity (I) was recorded in four independent runs of 30 s. When a peak in the scattering intensity was observed (Figure 4a), the titration was repeated with a delay time of 300 s to check that the appearance of the peak was not caused by slow processes taking place during the titration. Second-order cumulant analysis (standard ALV software) of the intensity autocorrelation functions ($g_2(\tau)$) yielded the characteristic decay rates (Γ), from which apparent diffusion coefficients (D) were calculated. Diffusion coefficients were converted to apparent hydrodynamic radii (R_h) using the Stokes−Einstein equation. The values of I and R_h after each addition were averaged, as were the intensity autocorrelation functions. The inverse Laplace transformation of the average $g_2(\tau)$, performed by CONTIN software (AfterALV 1.0d, Dullware), was used to analyze the size distributions of the C3Ms.

The total salt concentration (c_s) after each addition was calculated as the sum of added NaCl, counterions present in the solid polymer, and ions from the added acid and base. Scattering intensities were corrected for solvent scattering and variation in the solvent refractive index and normalized by the acrylic acid monomer concentration. From a plot of I/c_{AA} against c_s, the critical salt concentration ($c_{s,cr}$) was estimated as follows. First, a baseline intensity (I_b) was established at high salt concentration as the average I/c_{AA} over at least 100 mM. Then, the intensity curve was tracked from high to low salt concentration. The critical salt concentration was taken as the first point i (i.e., the highest salt concentration) for which the average intensity of three subsequent points was more than twice the baseline intensity ($(^1/_3)\sum_{i-2}^{i}(I/c_{AA})_i > 2I_b$). This method was verified to yield reasonable estimations of $c_{s,cr}$ by a visual inspection of curves having a clear breakpoint (Supporting Information). Because the errors in the resulting critical salt concentrations arise mainly from the choice of the threshold intensity (here $2I_b$), these errors were estimated as the difference in $c_{s,cr}$ if a threshold of $3I_b$ was used.

To test the reversibility of the response of our C3Ms to salt, the inverse of a light-scattering salt titration was also performed for several C3Ms. In this so-called light-scattering dilution titration, water was titrated into a C3M solution with c_s = 0.70 M. The combined results of a salt and dilution titration for a mixture of PAA_{1728} and $PM2VP_{41}$-*b*-PEO_{204} are shown in the Supporting Information. Because I/c_{AA}, R_h, and $c_{s,cr}$ are approximately the same in both titrations, the C3Ms were concluded to be in or near thermodynamic equilibrium.

Dynamic and Static Light Scattering. Dynamic and static light scattering (DLS and SLS) measurements were performed on an ALV instrument equipped with an ALV7002 external correlator and a 300 mW Cobolt Samba-300 DPSS laser operating at a wavelength of 532 nm. Unless specified otherwise, the samples were contained in 2.5-cm-diameter quartz cells (Hellma). To evaluate the angular dependence of $g_2(\tau)$ and the Rayleigh ratio (R), the scattering intensity was recorded at 15° ≤ θ ≤ 145° in intervals of 2°, in eight independent runs of 150 s (DLS) or 30 s (SLS) per angle. Using toluene as a reference, we calculated the Rayleigh ratio at each measured angle according to

$$R(\theta) = \frac{I_{sample}(\theta) - I_0(\theta)}{I_t(\theta)} \times R_t \times \left(\frac{n_0}{n_t}\right)^2 \quad (1)$$

where $I_{sample}(\theta)$, $I_0(\theta)$, and $I_t(\theta)$ are the sample, solvent, and toluene scattering intensities, respectively. R_t = 2.10 × 10^{-5} cm^{-1} is the Rayleigh ratio of toluene at λ = 532 nm,[34] and n_t = 1.496 is the refractive index of toluene.[35] $I_0(\theta)$ was approximated by $I_0(90)/\sin\theta$ because the scattering volume is proportional to $1/\sin\theta$. The validity of this approximation was confirmed by the fact that the measured values of $I_t(\theta)$ were fitted well by a $1/\sin\theta$ dependence. The detector dark current was at most 1% of the solvent and toluene scattering intensity and was therefore neglected. Rayleigh ratios were normalized by the polymer concentration, expressed as c_{AA}, and the optical constant (K)

$$K = \frac{4\pi^2 n_0^{\,2}(dn/dC)^2}{\lambda^4 N_{Av}} \quad (2)$$

where $n_0 = 1.3332 + 0.0096c_{NaCl}$ is the solvent refractive index for c_{NaCl} in M[35] and N_{Av} is Avogadro's number. dn/dC is the specific refractive index increment of the C3Ms, which was approximated by a weighted average of the refractive index increments of the polymeric components:[36] 0.261 mL/g for PAA,[37] 0.270 mL/g for PM2VP,[37] and 0.138 mL/g for PEO.[36] PAA and PM2VP were assumed to be fully charged, and the refractive index increment of PM2VP was approximated by that of P2VP. This gives a typical dn/dC of 0.197 mL/g for $PAA_{139}/PM2VP_{41}$-*b*-PEO_{204}. Finally, scattering angles were converted to scattering vectors (q) according to

$$q = \frac{4\pi n_0}{\lambda}\sin\left(\frac{\theta}{2}\right) \quad (3)$$

Determination of the Rotational Diffusion Coefficient. To determine the rotational diffusion coefficient (D_r) of the asymmetric objects present in an 8.8 mM $PAA_{13}/PM2VP_{41}$-*b*-PEO_{204} solution with c_s = 180 mM, we performed DLS measurements at different detection angles and analyzed them with CONTIN. All decay rate distributions at 67° ≤ θ ≤ 145° showed two modes: a large-amplitude mode at low Γ (Γ_{slow}) corresponding to translational diffusion and a small-amplitude mode at high Γ (Γ_{fast}) corresponding to a composite of translational and rotational motion. The latter mode can be written as a first-order approximation:[38]

$$\Gamma_{fast} = 6D_r + q^2 D_t \quad (4)$$

To estimate D_r, we plotted Γ_{fast} against q^2 and linearly extrapolated it to q^2 = 0 using the data for 67° ≤ θ ≤ 83°.

Depolarized Static Light Scattering. To measure depolarized light scattering intensities, a Glan-Laser prism polarizer (Melles Griot, 03 PGL 301/A, extinction ratio <5 × 10^{-5}) was placed in front of the detector. This polarizer could be adjusted to transmit only light with polarization perpendicular to the laser polarization (I^{vh}) or parallel to it (I^{vv}), allowing the determination of the depolarization ratio[39]

$$\Delta^{vh} = \frac{I^{vh} - I_0^{\,vh}}{I^{vv} - I_0^{\,vv}} \quad (5)$$

where I_0 denotes the solvent scattering intensity. Because the value of I^{vh} is very low, the scattering intensity in the absence of a polarizer ($I^{vu} = I$) is almost equal to I^{vv} (<0.001% difference). The error introduced by replacing the denominator in eq 5 with $I^{vu} - I_0^{\,vu}$ is much smaller than the error due to changing the orientation of the polarizer from 0 to 90° and vice versa, which is needed to measure both I^{vh} and I^{vv}. Therefore, I^{vv} and $I_0^{\,vv}$ were approximated by I^{vu} and $I_0^{\,vu}$. The samples were contained in 1-cm-diameter glass tubes with 0.85-mm-thick walls. For each sample, the scattering intensity was recorded at an angle of 55° in 10 independent runs of 30 s. θ = 55° was chosen instead of θ = 90° because the amount of depolarized light relative to the polarizer leakage increases with increasing separation from θ = 90°. Angles

dx.doi.org/10.1021/la303211b | *Langmuir* 2012, 28, 14180−14191

smaller than 55° were considered to be less suitable in this case because the lens effect due to the tube curvature also increases with increasing separation from $\theta = 90°$, resulting in increased distortion of the scattered light.

Critical Scattering. To investigate if critical scattering could explain the increases in intensity and hydrodynamic radius close to the critical salt concentration, SLS measurements were performed on PAA_{13}/$PM2VP_{41}$-*b*-PEO_{204} solutions with five different salt concentrations (c_s = 10, 100, 150, 180, and 200 mM). These samples were made by adding different amounts of a 1.0 M NaCl solution to a 4.4 mM PAA_{13}/$PM2VP_{41}$-*b*-PEO_{204} solution with c_s = 10 mM to obtain the same dilution factors as in the DLS salt titrations. For each salt concentration, the normalized Rayleigh ratio ($R(q)/Kc_{AA}$) was plotted as a function of q^2. The values of $R(q)/Kc_{AA}$ in the limit of $q \to 0$ were estimated by linear extrapolation of $R(q)/Kc_{AA}$ in the range of $15° \leq \theta \leq 25°$ to $q^2 = 0$. The obtained values of $R(0)/Kc_{AA}$ were plotted against the separation from the critical salt concentration ($c_{s,cr} - c_s$) on a double-logarithmic scale.

Small-Angle X-ray Scattering. Small-angle X-ray scattering (SAXS) experiments were performed at the European Synchrotron Radiation Facility (ESRF) in Grenoble, France, at the ID02 high brilliance beamline. An X-ray energy of 12.46 keV and two sample-to-detector distances of 1.5 and 3.0 m were used to cover a q range of $5.5 \times 10^{-2} < q < 3.0$ nm^{-1}. The samples were contained in polycarbonate capillaries (Enki SRL) of 1.9 mm diameter and maintained at a temperature of 20 ± 1 °C. The scattering data were corrected for background scattering, detector response, and primary beam intensity fluctuations. The instrument scattering vector was calibrated using a silver behenate standard.

All scattering curves were analyzed using SASfit software. The SAXS data of PAA_{13}/$PM2VP_{41}$-*b*-PEO_{204} at c_s = 180 mM were fitted to a form factor of a polydisperse flexible cylinder. The combined SLS and SAXS data of PAA_{13}/$PM2VP_{41}$-*b*-PEO_{204} at c_s = 10 mM and those of PAA_{139}/$PM2VP_{41}$-*b*-PEO_{204} at c_s = 280 mM were fitted to a form factor of a polydisperse core–shell sphere. Additional details of the fitting procedures and the values of the fitting parameters are provided in the Supporting Information. In all experiments, the polymer concentration (4.64 g/L) was low enough to neglect interactions between micelles, that is, the structure factor $S(q) \approx 1$.

Theoretical Calculation of Critical Salt Concentrations. The salt stability of C3Ms is predominantly determined by the strength of the polyelectrolyte complex that constitutes the core.[14] To calculate theoretical critical salt concentrations, the C3M core was modeled as a macroscopic complex between homopolyelectrolytes PAA and PM2VP. The process of polyelectrolyte complexation has been described in detail by Overbeek and Voorn.[31] We previously applied this mean-field lattice model successfully to describe experimental binodal compositions of mixtures of homopolyelectrolytes PAA and poly(*N*,*N*-dimethylaminoethyl methacrylate) (PDMAEMA). A full description of the parameters, calculations, assumptions, and limitations has been given elsewhere.[40] In this study, the same model was used, with two modifications to the parameters: the polyelectrolyte charge densities were adjusted to 1 instead of 0.95, and the chain lengths (N) were matched to the experimentally used PAA and PM2VP lengths. Calculated volume fractions were converted to molar concentrations using an empirical lattice size (l) of 0.65 nm to obtain good agreement with our experimental salt and polymer concentrations. For each combination of PAA_m and $PM2VP_n$, the critical salt concentration was obtained from the maximum of the corresponding binodal.

RESULTS AND DISCUSSION

Characterization of C3Ms. We have prepared C3Ms from different combinations of PAA_m and $PM2VP_n$-*b*-PEO_o. The corresponding hydrodynamic radii (R_h) at c_s = 10 mM are shown in Figure 2a as a function of the PAA chain length (N_{PAA}) for three different diblock copolymers. The first observation is that the size of the micelles increases with increasing PM2VP length (N_{PM2VP}). This is in agreement with

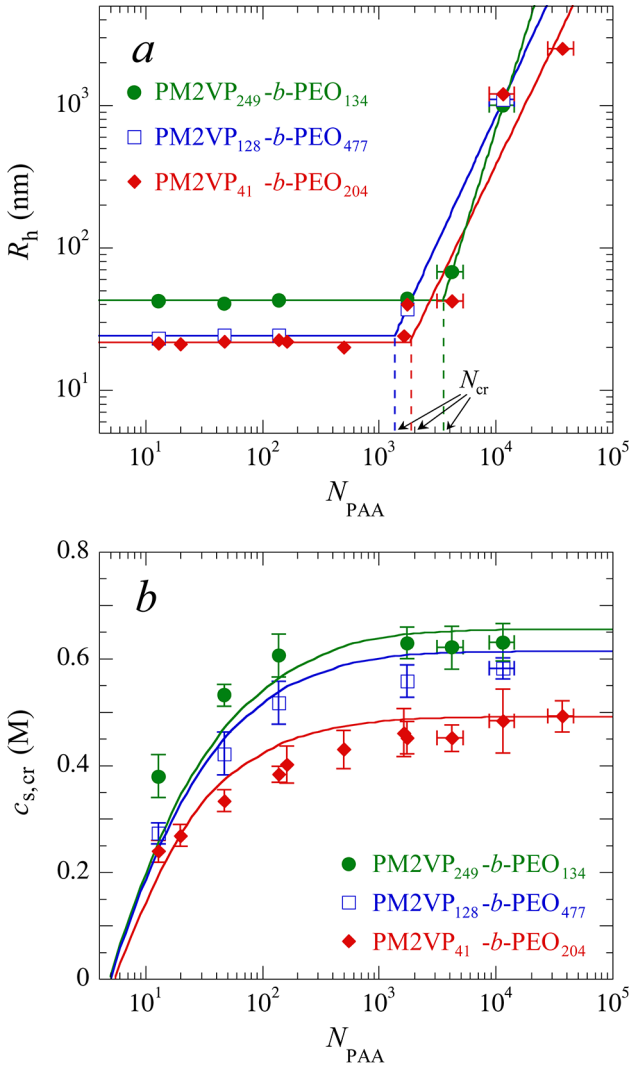

Figure 2. (a) Hydrodynamic radii of C3Ms of PAA and PM2VP-*b*-PEO at c_s = 10 mM as a function of the PAA chain length, as determined from DLS. The critical PAA lengths (N_{cr}) are estimated from the intersection points of the horizontal lines representing a constant radius at small N_{PAA} with the power-law fits at large N_{PAA}. Details of the fitting procedure are given in the Supporting Information. (b) Critical salt concentrations of the same C3Ms, as obtained from LS salt titrations (symbols) or as predicted from Voorn–Overbeek theory (solid lines). In all titrations, c_{AA} at the critical salt concentration was between 0.7 and 2.7 mM.

scaling theories that predict that both the radius of the core (R_{core}) and the thickness of the corona (H_{corona}) become larger with increasing length of the core-forming block because of an increase in the micellar aggregation number (P).[41] The length of the corona-forming block (here N_{PEO}) has only a small effect on the hydrodynamic radius of the micelles. It has been predicted[41,42] and found[25,41,43] that the overall micellar size increases slightly with increasing length of the corona-forming block. Figure 2a confirms that the PM2VP length has a greater influence on R_h than does the PEO length: although $PM2VP_{249}$-*b*-PEO_{134} has a shorter PEO block than the other two diblock copolymers, its very long PM2VP block gives rise to C3Ms with the largest overall size. C3Ms formed from $PM2VP_{128}$-*b*-PEO_{477} are somewhat larger than C3Ms formed from $PM2VP_{41}$-*b*-PEO_{204}, consistent with the fact that both its PM2VP and PEO blocks are longer.

dx.doi.org/10.1021/la303211b | *Langmuir* 2012, 28, 14180–14191

A second observation from Figure 2a is that a "critical" PAA length (N_{cr}) exists for each diblock copolymer. For $N_{PAA} < N_{cr}$, the hydrodynamic radius is approximately constant, whereas for $N_{PAA} > N_{cr}$, it increases sharply with increasing N_{PAA}. We estimate the critical PAA lengths from the intersection points between the horizontal and power-law trend lines in Figure 2a (Supporting Information). This gives $N_{cr} = 1.4 \times 10^3$, 1.9×10^3, and 3.5×10^3 for PM2VP$_{128}$-*b*-PEO$_{477}$, PM2VP$_{41}$-*b*-PEO$_{204}$, and PM2VP$_{249}$-*b*-PEO$_{134}$, respectively. Assuming an error of 0.4×10^3 (Supporting Information), we conclude that the difference in N_{cr} between the first two diblock copolymers is negligible. PM2VP$_{249}$-*b*-PEO$_{134}$, however, has a considerably larger critical PAA length. We believe that this is due to the higher aggregation number of PAA$_m$/PM2VP$_{249}$-*b*-PEO$_{134}$, as we will explain below.

A similar dependence of the C3M size on the homopolymer chain length was reported by Van der Burgh et al.[25] They attributed the increase in the hydrodynamic radius above N_{cr} to the limited volume of the micellar core (Figure 1a). For $N_{PAA} < N_{cr}$, the total number of monomers in the core is independent of N_{PAA} and equal to $2N_{cr}$, but when the length of a single PAA chain exceeds N_{cr}, the core can no longer accommodate an entire PAA chain without growing in size. As a result, both the aggregation number and the hydrodynamic radius of the micelles increase. Because C3Ms of PM2VP$_{249}$-*b*-PEO$_{134}$ and short PAA chains have an aggregation number that is greater than that of C3Ms of the other two diblock copolymers, their core can accommodate more PAA monomers, resulting in a larger critical PAA length.

Above N_{cr}, C3Ms are probably coassemblies of a single PAA chain and N_{PAA}/N_{PM2VP} diblock copolymer chains. However, the term C3M may not be appropriate for coassemblies with $N_{PAA} \gg N_{cr}$ because their hydrodynamic radii exceed the PM2VP-*b*-PEO contour lengths (estimated to be $L_c \approx 0.26N_{PM2VP} + 0.40N_{PEO}$ nm,[44,45] which amounts to 90 nm for PM2VP$_{41}$-*b*-PEO$_{204}$, 220 nm for PM2VP$_{128}$-*b*-PEO$_{477}$, and 120 nm for PM2VP$_{249}$-*b*-PEO$_{134}$). Because the PM2VP blocks cannot reach the center of these coassemblies, the core is not a homogeneous complex coacervate. The radii of some of these structures are even larger than expected for single high-M_w PAA chains, which suggests that secondary aggregation has occurred. From depolarized light-scattering measurements, we know that these structures are spherically symmetric and are not ellipsoidal or wormlike micelles (data not shown).

The hydrodynamic radii of C3Ms of PM2VP$_{41}$-*b*-PEO$_{204}$ and PM2VP$_{249}$-*b*-PEO$_{134}$ below N_{cr} (22 ± 2 and 42 ± 2 nm, respectively) are in good agreement with literature values. Danial et al. reported $R_h = 23 \pm 3$ nm for PAA$_{48}$/PM2VP$_{41}$-*b*-PEO$_{204}$ in 50 mM $NaNO_3$ at pH 7.7.[29] Both Lindhoud et al. and Brzozowska et al. measured a hydrodynamic radius of 22 nm for PAA$_{139}$/PM2VP$_{41}$-*b*-PEO$_{204}$ at pH 7.1 in 3.5 mM sodium phosphate buffer and water, respectively.[30,11] Guragain et al. reported for C3Ms of PMAA$_{139}$ (poly(methacrylic acid)) and PM2VP$_{249}$-*b*-PEO$_{134}$, which are very similar to PAA$_{139}$/PM2VP$_{249}$-*b*-PEO$_{134}$, that $R_h = 37 \pm 3$ nm under charge stoichiometric conditions in water.[46] Reports on PAA$_m$/PM2VP$_{128}$-*b*-PEO$_{477}$ are lacking.

A final, surprising observation is the large difference in size between PAA$_{1630}$/PM2VP$_{41}$-*b*-PEO$_{204}$ (R_h = 24 nm) and PAA$_{1728}$/PM2VP$_{41}$-*b*-PEO$_{204}$ (R_h = 40 nm) in Figure 2a. We attribute this to the different polydispersity indices of PAA$_{1630}$ and PAA$_{1728}$, which are 1.60 and 1.25, respectively. Because N_{cr} is around 1.9×10^3, a single PAA$_{1630}$ or PAA$_{1728}$ chain is not sufficient to form a stable micelle. It has to be combined with a very short PAA chain to reach 1.9×10^3 total monomers. Alternatively, two intermediately long chains with $N_{PAA} \approx 1 \times 10^3$ or a single PAA$_{1900}$ chain can be incorporated. The relatively high polydispersity of PAA$_{1630}$ allows all three scenarios. The sample with PAA$_{1728}$, however, has a narrower distribution of PAA lengths. These C3Ms must probably incorporate two longer PAA chains and are therefore larger.

Stability of C3Ms. When salt is added to a solution of C3Ms, the cmc increases, resulting in the disassembly of C3Ms. We here define the stability of C3Ms as their ability to resist this salt-induced disintegration. We express stability quantitatively by means of the critical salt concentration ($c_{s,cr}$), which is the salt concentration at which the cmc equals the polymer concentration and all C3Ms are disintegrated. A well-established method of studying the salt stability of C3Ms is a light-scattering (LS) salt titration.[21,47] Because the disassembly of micelles causes a decrease in the scattering intensity, the critical salt concentration can be directly estimated from the break point in a plot of scattering intensity versus salt concentration. To answer our first question about the effect of the polymer chain length on the salt stability of C3Ms, we have performed LS salt titrations for the same set of C3Ms as studied in the previous section. Their critical salt concentrations are shown as symbols in Figure 2b.

For each diblock copolymer, we find that the critical salt concentration increases with increasing PAA length and levels off for long PAA chains. Increasing the PM2VP block length also leads to improved salt stability of the C3Ms, an effect that seems to become less pronounced for longer PM2VP blocks. We notice a striking similarity between these trends and the chain-length dependence of $c_{s,cr}$ for macroscopic complex coacervates.[40] Apparently, the same forces that drive the complexation of two oppositely charged homopolyelectrolytes drive the formation of the C3M core. Following this hypothesis, we have modeled the C3M core as a macroscopic complex between PAA and PM2VP. Theoretical predictions of $c_{s,cr}$ are depicted by solid lines in Figure 2b. Indeed, we find quite good agreement with our experimental results using only the effective lattice size (l) as an adjustable parameter. Only for complexes of PM2VP$_{249}$ and short PAA chains are the critical salt concentrations of the C3Ms considerably higher than those predicted for macroscopic complex coacervates. We conclude from this that the PEO blocks also affect the salt stability of C3Ms because of steric repulsion between the solvated PEO blocks.

We explain the observed dependence of $c_{s,cr}$ on N_{PAA} from the equation that forms the basis of our calculations. According to Overbeek and Voorn, the total free energy (F) of a polyelectrolyte solution is the sum of the Debye–Hückel electrostatic free energy, which favors associative phase separation, and the Flory–Huggins entropy of mixing, which favors random mixing[31]

$$\frac{F}{Mk_BT} = -\alpha\left(\sum_i \sigma_i\phi_i\right)^{3/2} + \sum_i \frac{\phi_i}{N_i}\ln\phi_i \qquad (6)$$

where σ_i, ϕ_i, and N_i are the charge density, volume fraction, and number of repeat units, respectively, of component i. M is the number of lattice sites, and α is a tuning parameter for the strength of the electrostatic interactions.[40] The first term in this equation, representing the electrostatic free energy, is independent of chain length because the Debye–Hückel

approximation neglects the connectivity of the charges along the polymer chains. The second term, corresponding to the mixing entropy, is proportional to $^1/_N$, and hence long polymer chains have a stronger tendency to phase separate than short chains. This explains why the salt stability improves with increasing N_{PAA} and N_{PM2VP}. For very long chains, the entropy of mixing becomes negligible, which thus leads to a leveling off of the critical salt concentrations.

An experimental parameter that we have not taken into account yet is the polymer concentration. As we mentioned above, the critical salt concentrations that we show in Figure 2b are the salt concentrations at which the total polymer concentration equals the critical micelle concentration. Because the cmc of C3Ms increases exponentially with the square root of the salt concentration, we expect to find higher critical salt concentrations at higher polymer concentrations.[13,14] To assess the importance of this concentration dependence in our experiments, we have performed LS salt titrations for different initial polymer concentrations. We indeed find an exponential dependence of the cmc on the square root of the salt concentration (Supporting Information), but the polymer concentrations in our titrations were sufficiently high to ensure a negligible dependence of $c_{s,cr}$ on c_{AA}.

Morphology of C3Ms. Now that we know the effect of the polymer chain length on the salt stability of C3Ms and on their size at low salt concentration, we will study the effect of the homopolymer length on the morphology of C3Ms with increasing salt concentration. By the term morphology we refer to both the size and shape of the micelles. We focus on C3Ms formed from PM2VP$_{41}$-*b*-PEO$_{204}$ and various PAA homopolymers (PAA$_{13}$-PAA$_{1728}$), thus not considering the aggregated structures with $N_{PAA} \gg N_{cr}$.

Size. The effect of salt on the size of C3Ms is far from trivial. In the existing literature, both increasing and decreasing hydrodynamic radii with increasing salt concentration have been reported. The salt-induced growth of C3Ms is usually attributed to the swelling of the core as a result of solvent uptake.[13,48] An equivalent shrinkage is typically attributed to a decrease in the aggregation number (P) as a result of reduced core−solvent interfacial tension.[27,30] Although both proposed mechanisms have been experimentally verified for macroscopic coacervates[40,49] and the decrease in the aggregation number also for C3Ms,[13,14] it is unclear what causes the discrete distinction between growing and shrinking of C3Ms. From a report by Lindhoud et al., it could be inferred that the effect of salt depends on the homopolymer chain length: whereas C3Ms containing the small lysozyme protein were found to grow upon addition of salt, salt-induced shrinkage of the C3Ms was observed when the lysozyme was partially replaced by the larger PDMAEMA$_{150}$ homopolymer.[2]

To investigate if the homopolymer length has a systematic effect on the size of C3Ms, we have performed dynamic light scattering (DLS) salt titrations for combinations of PM2VP$_{41}$-*b*-PEO$_{204}$ and various PAA homopolymers. Figure 3 shows the mean apparent hydrodynamic radii of these C3Ms as a function of salt concentration. We indeed find a systematic effect of the PAA length on the size of PAA$_m$/PM2VP$_{41}$-*b*-PEO$_{204}$: micelles with $N_{PAA} \leq 47$ grow upon addition of salt whereas micelles with $N_{PAA} \geq 139$ shrink. A close inspection of the corresponding intensity curves reveals that the increase in size is always accompanied by a peak in the scattering intensity. Figure 4 shows the normalized light-scattering intensity (I/c_{AA}) of mixtures of PM2VP$_{41}$-*b*-PEO$_{204}$ and (a) PAA$_{13}$ or (b) PAA$_{139}$

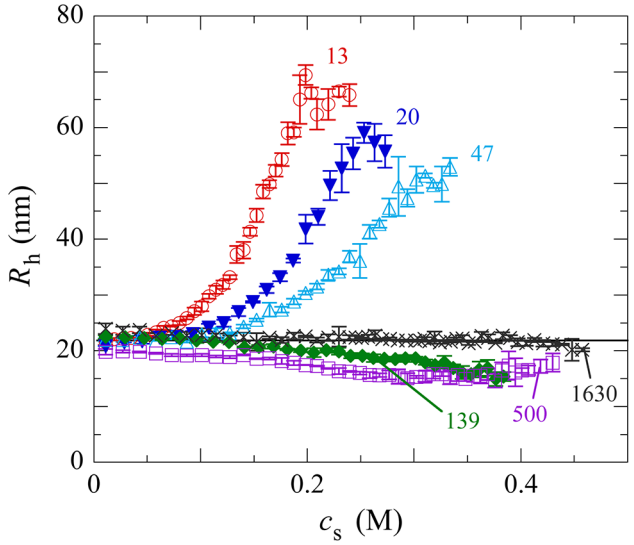

Figure 3. Mean apparent hydrodynamic radii of C3Ms of PM2VP$_{41}$-*b*-PEO$_{204}$ and PAA with N_{PAA} = 13, 20, 47, 139, 500, and 1630 as a function of salt concentration. Only data points up to the critical salt concentrations are shown. The symbols are averages of four independent runs, with the error bars representing the standard deviations. The solid horizontal line indicates the average R_h at c_s = 10 mM. The initial polymer concentration (c_{AA}) was 1.1 mM in all titrations.

as a function of salt concentration. For both PAA lengths, the intensity initially decreases linearly with increasing salt concentration, but for PAA$_{13}$/PM2VP$_{41}$-*b*-PEO$_{204}$, a very distinct peak is observed just before the critical salt concentration. This intensity peak is absent for all concentrations of PAA$_{139}$/PM2VP$_{41}$-*b*-PEO$_{204}$.

A peak in scattering for C3Ms upon addition of salt has been observed by several other authors.[13,15,20−22,28] According to Lindhoud et al., the increase in scattering intensity is caused by structural changes in the corona.[21] Soliman attributes it to the fusion of C3Ms into larger structures as a result of the partial dehydration of the PEO corona.[22] In the report of Gaucher et al., the presence of an intensity peak seems to depend on the homopolymer length, similar to what we find. For C3Ms containing poly(L-lysine) (pLys) as a homopolymer, they observed a peak only for N_{pLys} = 13 and not for N_{pLys} = 57 and 207.[15]

In our salt titrations on PAA$_{13}$/PM2VP$_{41}$-*b*-PEO$_{204}$, the increase in scattering clearly originates from the formation of larger objects ($R_h \approx 70$ nm, see Figure 3). These structures are not merely "swollen" C3Ms because swelling would imply a decrease in the core density and contrast, leaving the scattering intensity virtually unchanged. They must have a higher aggregation number. We believe that these objects are no longer spherical micelles, because the size of the diblock copolymer does not allow for such large hydrodynamic radii, but instead they are elongated, wormlike micelles (Figure 1b). At higher polymer concentrations, these wormlike micelles grow longer:[50] when the polymer concentration is increased from 1.1 to 4.4, 6.6, and 8.8 mM, we find an increase in not only the peak height of the scattering intensity (Figure 4a) but also in the corresponding apparent hydrodynamic radii (from 69 to 82, 90, and 102 nm, data not shown).

CONTIN analysis of solutions of PAA$_{13}$/PM2VP$_{41}$-*b*-PEO$_{204}$ (Figure 5a) reveals that a bimodal size distribution underlies

dx.doi.org/10.1021/la303211b | *Langmuir* 2012, 28, 14180−14191

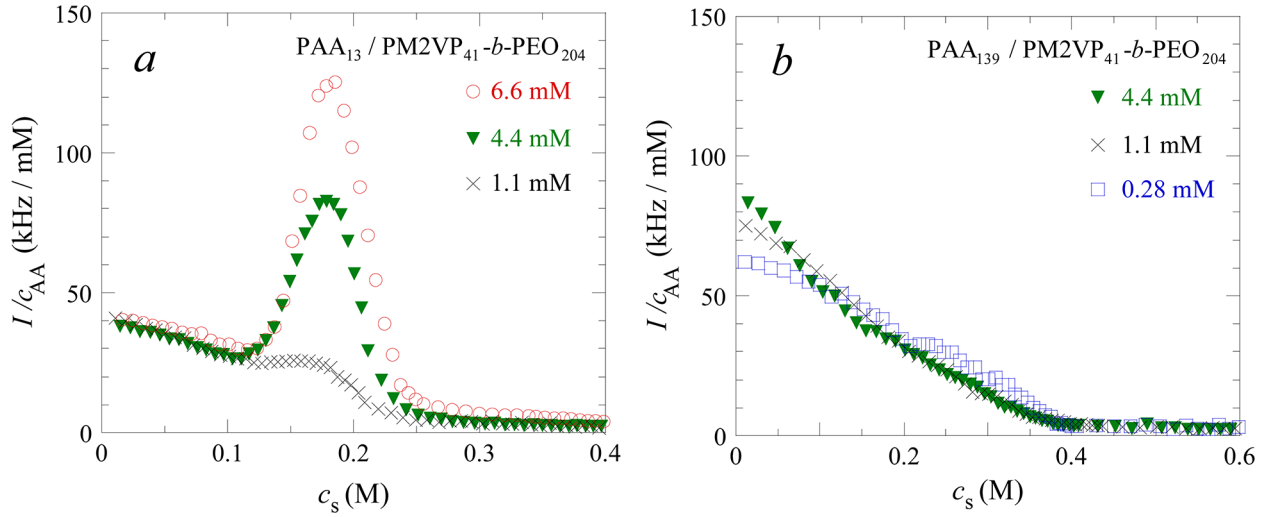

Figure 4. Light-scattering intensity, normalized by the acrylic acid monomer concentration, as a function of salt concentration for mixtures of $PM2VP_{41}$-*b*-PEO_{204} and (a) PAA_{13} or (b) PAA_{139}. The symbols are averages of four independent runs. The initial polymer concentrations are indicated by the labels.

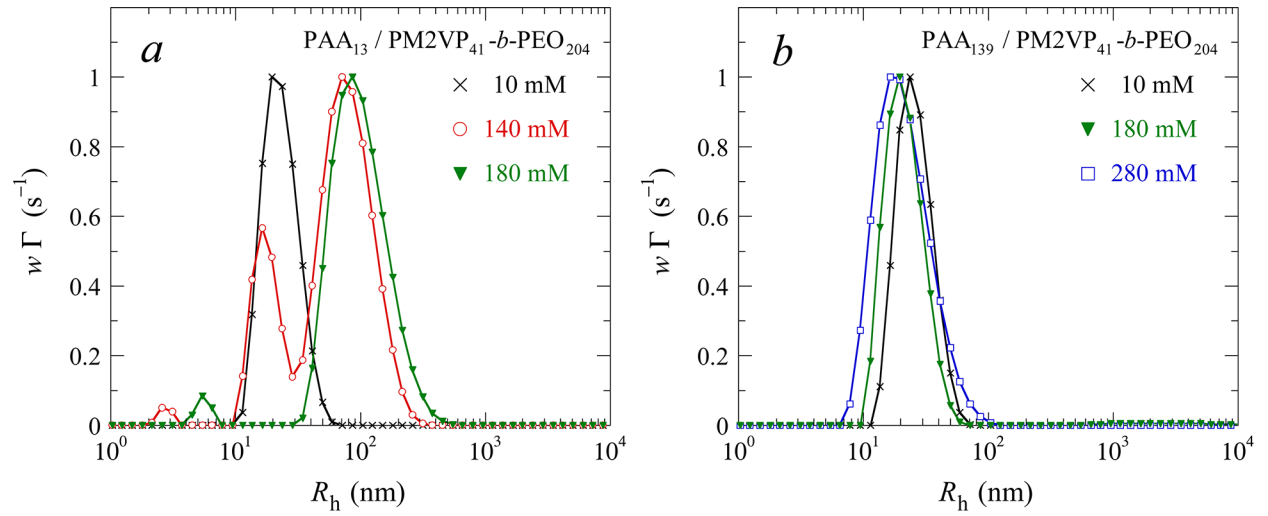

Figure 5. CONTIN size distributions for mixtures of $PM2VP_{41}$-*b*-PEO_{204} and (a) PAA_{13} or (b) PAA_{139} at different salt concentrations, as indicated by the labels. The polymer concentration ranged from c_{AA} = 4.4 mM at c_s = 10 mM to 3.2 mM at c_s = 280 mM. All distributions are normalized to the maximum of the highest mode. Because w is proportional to R^6 and Γ is proportional to $^1/_R$, the correction factor for obtaining a number average is $^1/_{R^5}$.

the apparent growth we observe in Figure 3. With increasing salt concentration, large objects with a hydrodynamic radius close to 100 nm grow at the expense of small micelles with $R_h \approx 20$ nm. This bimodal distribution is independent of the fitting parameters. By contrast, $PAA_{139}/PM2VP_{41}$-*b*-PEO_{204} has a unimodal size distribution at all salt concentrations, which clearly shows the shrinkage of the micelles (Figure 5b). Interestingly, the radius of the spherical micelles in the $PAA_{13}/PM2VP_{41}$-*b*-PEO_{204} solution also decreases slightly with increasing salt concentration (Figure 5a). The polydispersity of both $PAA_{13}/PM2VP_{41}$-*b*-PEO_{204} and $PAA_{139}/PM2VP_{41}$-*b*-PEO_{204} increases upon addition of salt, as has been found previously for C3Ms.[13,14]

Shape. How can we support the hypothesis that wormlike C3Ms are formed with increasing salt concentration? Unfortunately, direct visualization techniques, such as (cryogenic) transmission electron microscopy ((cryo-)TEM) and atomic force microscopy (AFM) imaging, are subject to several difficulties, limitations, and interpretation issues when applied to C3M systems. C3Ms are known to adsorb on most surfaces, followed by spreading and dissociation,[10] which makes the study of their shape in solution impossible by TEM and AFM. With cryo-TEM, the shape in solution is frozen and then studied, but the small difference in electron density between the core and the surrounding solution makes the observation of the core difficult. In previous cases where cryo-TEM was used to visualize C3Ms, metal ions in the cores of the C3Ms often provided the necessary contrast.[13,14]

Instead, we use a combination of various scattering techniques to support our hypothesis. These techniques allow in situ characterization of C3Ms in solution without the need for contrast agents. First, we measure the rotational diffusion coefficient (D_r) of the large objects by dynamic light scattering. CONTIN analysis of the intensity autocorrelation function ($g_2(\tau)$) for different samples reveals that in all cases where we find these large objects we also find a small-amplitude mode at

dx.doi.org/10.1021/la303211b | *Langmuir* 2012, 28, 14180−14191

very low R_h (e.g., Figure 5a). The decay rate of this "fast" mode (Γ_{fast}) does not correspond to purely translational diffusion of C3Ms. Instead, we argue that it corresponds to a combination of rotational and translational motion of the large objects, following the reasoning of Schillén et al.[38] This fast mode is observed only for asymmetric structures that have a detectable rotational diffusion coefficient, such as wormlike micelles. The magnitude of Γ_{fast} depends on the scattering vector (q) and on the size and shape of the asymmetric objects. In Figure 6a, we show a plot of Γ_{fast} and Γ_{slow} versus q^2 for an 8.8 mM PAA_{13}/$PM2VP_{41}$-*b*-PEO_{204} solution with c_s = 180 mM. Following the example of Schillén et al., we extrapolate Γ_{fast} to $q^2 = 0$ and find that $D_r = 1.8 \times 10^3$ s^{-1}.

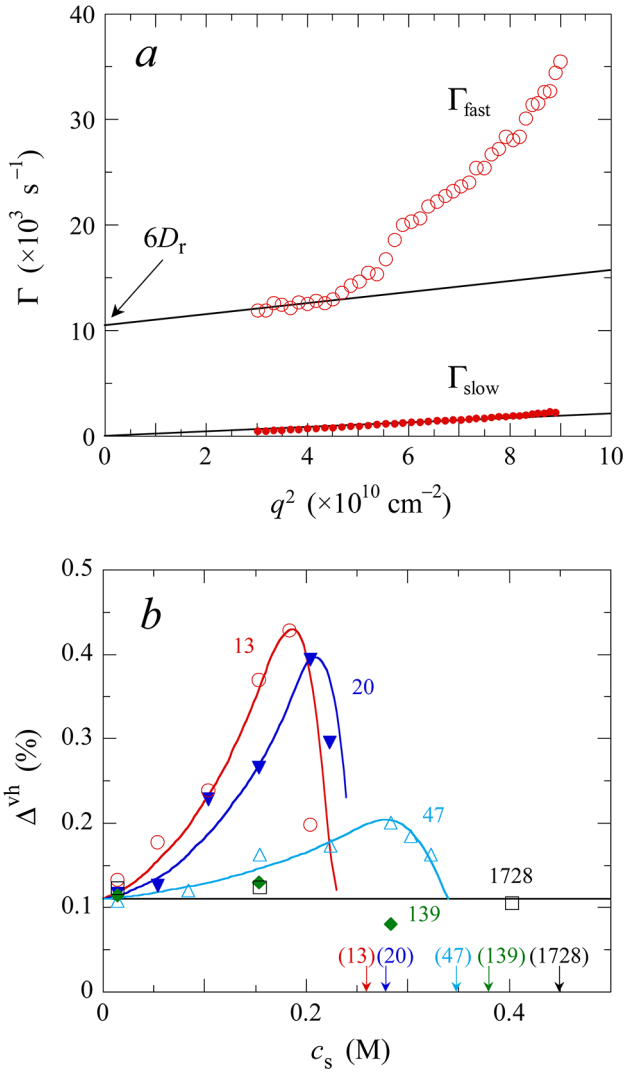

Figure 6. (a) Fast and slow decay rates of the intensity autocorrelation function versus q^2 for mixtures of $PM2VP_{41}$-*b*-PEO_{204} and PAA_{13} at c_s = 180 mM and c_{AA} = 8.8 mM. The symbols are averages over eight independent runs. The upper solid line is a linear fit to the data points of Γ_{fast} at $3.0 \times 10^{10} < q^2 < 4.3 \times 10^{10}$ cm^{-2}, for which the intercept with the ordinate equals $6D_R$. The lower solid line is a linear fit to all data points of Γ_{slow}. (b) Depolarization ratio (in %) as a function of salt concentration for mixtures of $PM2VP_{41}$-*b*-PEO_{204} and PAA with N_{PAA} = 13, 20, 47, 139, and 1728, as indicated by the labels. The symbols are averages over 10 independent runs. The solid lines are guides to the eye. The arrows point to the critical salt concentrations, as obtained from the LS salt titrations, with N_{PAA} indicated by the labels in parentheses.

The rotational diffusion coefficient can be expressed as a function of the length (L) and diameter (d) of the micelles. As an approximation, we use an equation for monodisperse rigid spherocylinders[51] (Supporting Information) in which we set d to twice the hydrodynamic radius of a spherical C3M ($R_h \approx 20$ nm) and use L as the fitting parameter. This procedure gives L = 130 nm and L/d = 3.3. Clearly, the order of magnitude is in agreement with the hydrodynamic radius obtained from the translational diffusion of these micelles ($2R_h \approx 200$ nm). A possible explanation for the discrepancy between the two values is that, in reality, wormlike micelles exhibit a significant polydispersity and flexibility so that the approximation of monodisperse rigid cylinders does not hold. In addition, the diameter of wormlike C3Ms may be smaller than that of spherical C3Ms, implying a longer contour length than calculated above.

A second confirmation of the presence of nonspherical particles in solutions of $PM2VP_{41}$-*b*-PEO_{204} and short PAA chains at high salt concentration comes from depolarized static light scattering measurements. Intensity associated with light that is polarized perpendicular to the incident light (I^{vh}) originates from particles with different polarizabilities parallel and perpendicular to their major axes ($\alpha_{\parallel} \neq \alpha_{\perp}$).[52] The depolarization ratio (Δ^{vh}, see eq 5) reflects the degree of optical anisotropy in solution, which scales with both the number and length of anisotropic particles. In Figure 6b, we show depolarization ratios as a function of salt concentration for mostly the same polymer combinations as in Figure 3. At c_s = 10 mM, Δ^{vh} is very small and approximately the same for all C3Ms, corresponding to a spherical morphology that is independent of PAA length. With increasing salt concentration, we find a clear increase in Δ^{vh} for C3Ms with short PAA chains, which also show an increase in size and polarized scattering intensity. The increase in Δ^{vh} is consistent with the formation of anisotropic particles such as wormlike micelles. By contrast, the depolarization ratio of C3Ms with long PAA chains remains approximately constant upon the addition of salt. Interestingly, Δ^{vh} seems to exhibit maxima at approximately the same salt concentrations where the maxima of the corresponding intensity peaks occur (e.g., Figure 4a). We also notice that the increase in Δ^{vh} is larger for N_{PAA} = 13 and 20 than for N_{PAA} = 47, which we attribute to the fact that C3Ms of PAA_{13} and PAA_{20} grow into longer worms than do C3Ms of PAA_{47} (Figure 3).

Third, we have performed a combination of static light scattering (SLS) and small-angle X-ray scattering (SAXS) to further confirm the wormlike morphology of C3Ms with short PAA chains at high salt concentration. Figure 7 shows the results of these experiments for C3Ms of $PM2VP_{41}$-*b*-PEO_{204} and (a) PAA_{13} or (b) PAA_{139} at different salt concentrations. The PEO corona contributes only marginally to the total scattering intensity because of its low polymer volume fraction.[30,43] For PAA_{13}/$PM2VP_{41}$-*b*-PEO_{204}, we observe a dramatic change in the shape of the scattering curve with increasing salt concentration. At c_s = 10 mM, the scattering intensity exhibits a clear plateau up to $q \approx 0.11$ nm^{-1} and then falls off as $I(q) \propto q^{-4}$, indicating that these micelles are spherical objects with a core size of ~9 nm. At c_s = 180 mM, however, the scattering intensity has a power-law slope of close to −1 in the range of $3 \times 10^{-2} < q < 6 \times 10^{-1}$ nm^{-1}. This slope is typical of cylindrical rods and wormlike chains on length scales

dx.doi.org/10.1021/la303211b | Langmuir 2012, 28, 14180−14191

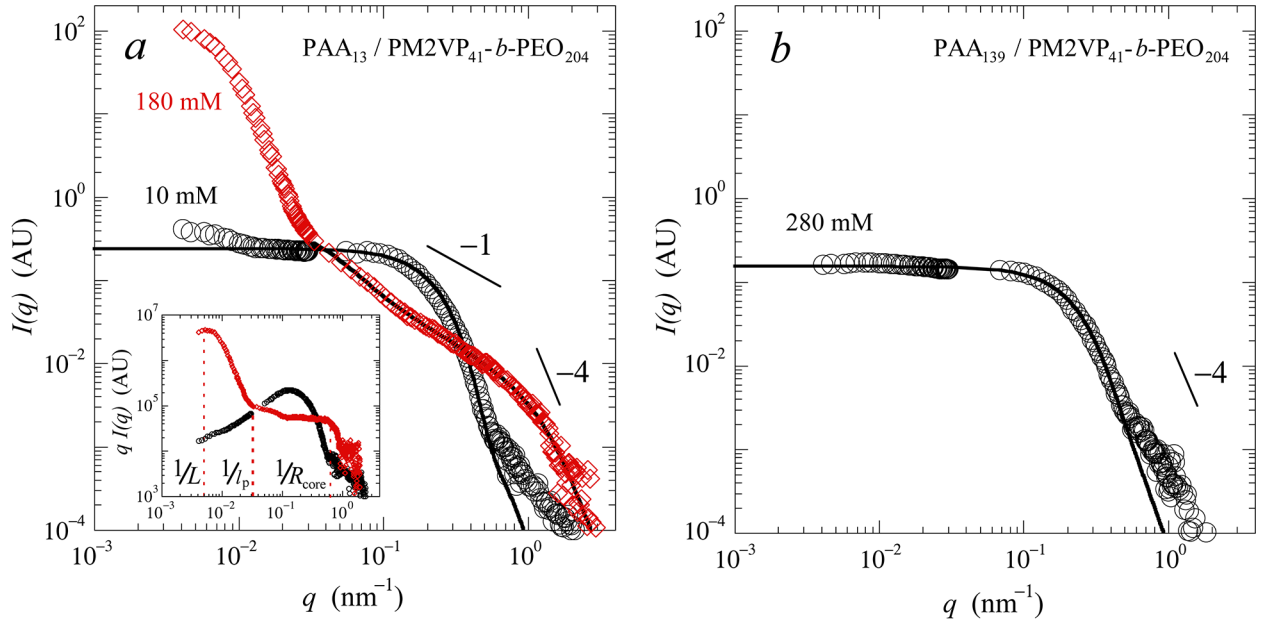

Figure 7. Combined SLS and SAXS measurements for C3Ms of PM2VP$_{41}$-*b*-PEO$_{204}$ and (a) PAA$_{13}$ or (b) PAA$_{139}$. The inset shows a Casassa−Holtzer representation of the data in plot a. The solid line in plot a for c_s = 10 mM and the solid line in plot b are fits to a form factor of a polydisperse (Gaussian distribution) core−shell sphere. The solid line in plot a for c_s = 180 mM is a fit to the form factor of a polydisperse (Gaussian distribution) flexible cylinder. c_{AA} was 8.8 mM in all experiments. Only 30% of the data points are shown.

between the cross-sectional radius of the rods (here R_{core}) and the persistence length (l_p).[50] We find a plateau at much lower q than for the spherical micelles, which here corresponds to the typical length (L) of the wormlike micelles. From the boundaries of these regimes, which can be identified in a so-called Casassa−Holtzer or bending-rod plot of $\log(qI(q))$ versus $\log q$[50] (inset of Figure 7a), we derive that $R_{core} \approx 1.5$ nm, which is significantly smaller than for spherical micelles, $l_p \approx 30$ nm, and $L \approx 250$ nm. These values are in good agreement with the values that we obtain from a fit of the data to a wormlike chain model (Supporting Information). We note that we have not been able to fit the low-q upturn with this model. Such an upturn with a power-law slope of close to −4 probably originates from a small fraction of larger aggregates.[53]

Figure 7b shows that wormlike micelles are not formed in a solution of PAA$_{139}$ and PM2VP$_{41}$-*b*-PEO$_{204}$. At c_s = 280 mM, which is rather close to the critical salt concentration, the scattering data are very similar to those of PAA$_{13}$/PM2VP$_{41}$-*b*-PEO$_{204}$ at c_s = 10 mM. We notice that distinct form factor minima are absent in all scattering curves. This indicates that the C3Ms have a significant polydispersity, as has been found before.[2,54] From fits of the scattering curves of PAA$_{13}$/PM2VP$_{41}$-*b*-PEO$_{204}$ at c_s = 10 mM and PAA$_{139}$/PM2VP$_{41}$-*b*-PEO$_{204}$ at c_s = 280 mM to the form factor of a polydisperse sphere, we find that the core radius of the former is 8.7 ± 2.5 nm and that of the latter is 5.4 ± 3.4 nm. We attribute the difference between these values to the fact that, upon addition of salt, the aggregation number of spherical C3Ms decreases,[6] resulting in a decrease in the core radius.[21,27,30] It has also been found that the polydispersity of C3Ms increases with increasing salt concentration.[13,14] Figure 5 confirms both trends and shows that the size and polydispersity of C3Ms of PAA$_{13}$ and PAA$_{139}$ at c_s = 10 mM are approximately the same. However, scattering data of PAA$_{139}$/PM2VP$_{41}$-*b*-PEO$_{204}$ at c_s = 10 mM are required to draw this conclusion unambiguously.

We can estimate the thickness of the corona (H_{corona}) of the spherical micelles from the difference between their hydrodynamic radius and core radius (Figure 1a). This gives for both PAA$_{13}$/PM2VP$_{41}$-*b*-PEO$_{204}$ at c_s = 10 mM and PAA$_{139}$/PM2VP$_{41}$-*b*-PEO$_{204}$ at c_s = 280 mM a corona thickness of ∼13 nm. Because both micelles have $R_{core} < H_{corona}$, they are in the so-called "starlike" regime. Interestingly, Zhulina et al. have reported that transitions between spherical and wormlike morphologies occur only for micelles that are in or close to the "crew-cut" regime ($R_{core} > H_{corona}$).[42] We argue that PAA$_{13}$/PM2VP$_{41}$-*b*-PEO$_{204}$ is closer to this regime than we conclude on the basis of its core and corona size. As has been found before, the core−corona interface of C3Ms is not well defined,[27,55] in contrast to that of micelles with a hydrophobic core-forming block as discussed by Zhulina et al. The core−corona interface of C3Ms shows a gradual transition from predominantly core-forming blocks to mainly corona-forming blocks. At the same time, the solvent volume fraction increases with increasing distance from the micelle center.[55] The radii obtained from the form factor fits are therefore only approximations of the core radii, and we cannot determine conclusively whether our C3Ms are in the starlike or crew-cut regime.

Critical Scattering. Finally, we investigate critical scattering as an alternative explanation for the observed peak in the scattering intensity and the apparent growth of C3Ms with short PAA chains upon addition of salt. Critical scattering has been reported for several micellar systems in the vicinity of a critical point and gives rise to increases in the scattering intensity and typical size.[56,57] It originates from critical fluctuations in concentration, which are enhanced as the critical point is approached.[58] In the reports mentioned above, the scattering intensity at q = 0 follows a critical power-law scaling of $I(0) \propto (T_{cr} - T)^{-1}$. Here, we approach the critical point by increasing the salt concentration. Figure 8 shows the normalized Rayleigh ratio in the limit of $q \rightarrow 0$ ($R(0)/Kc_{AA}$)

dx.doi.org/10.1021/la303211b | *Langmuir* 2012, 28, 14180−14191

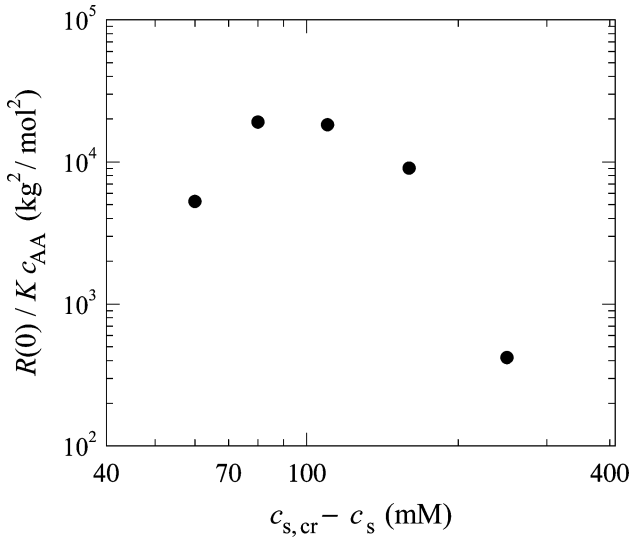

Figure 8. Analysis of critical scattering from C3Ms of PAA_{13} and $PM2VP_{41}$-*b*-PEO_{204}. The normalized Rayleigh ratio in the limit of $q \rightarrow 0$ is plotted as a function of the separation from the critical salt concentration ($c_{s,cr}$ = 260 mM). The polymer concentration (c_{AA}) ranged from 4.4 mM for c_s = 10 mM to 3.6 mM for c_s = 200 mM.

as a function of the separation from the critical salt concentration ($c_{s,cr} - c_s$) for mixtures of PAA_{13} and $PM2VP_{41}$-*b*-PEO_{204}. (See the Supporting Information for a plot of $R(q)/Kc_{AA}$ vs q^2.) We observe no critical scaling, from which we conclude that critical scattering does not underlie the increases in the hydrodynamic radii and scattering intensities in Figures 3 and 4a, respectively. These results provide further evidence for the formation of wormlike micelles.

Possible Mechanism of Wormlike Micelle Formation. We have found that C3Ms with short PAA chains can undergo a morphological transition from spherical to wormlike micelles upon addition of salt. We rationalize this transition using the concept of the packing parameter (p). This parameter is traditionally defined for amphiphilic molecules as $p = v_0/al_0$, with v_0 and l_0 being the volume and length of the hydrophobic tail, respectively, and a being the area of the hydrophilic headgroup.[59] We note that applying this concept to C3Ms is a rather crude and simplified approximation based on mean-field parameters that, in the case of flexible chains, are the result of an intricate interplay of several competing and fairly complicated contributions. Still, we find that the concept is effective at capturing the general trends. For our C3Ms, we assume that the PM2VP block, complexed with N_{PM2VP} AA monomers, plays the role of the hydrophobic tail. The area of the PEO block at the core−corona interface is the effective headgroup area. At low salt concentration, our C3Ms are spherical, implying that $p < {}^1/_3$. The effect of salt is twofold. First, it screens the electrostatic interactions between PAA and PM2VP, resulting in swelling of the complex and a consequent increase of v_0.[6] Second, it decreases the solubility of PEO, causing the PEO blocks to become more compact and thereby decreasing a.[60] Both lead to an increase of the packing parameter, which promotes the formation of structures with lower curvature such as wormlike micelles.

The question now arises: why are these wormlike micelles not formed for long PAA homopolymers? We believe that this can be explained by the fact that long PAA chains must interact with multiple PM2VP blocks. An increase in the packing parameter requires an increase in separation between the PM2VP blocks that are complexed with segments of the PAA chains. Because sufficiently short PAA homopolymers interact with only one PM2VP block, the C3Ms of these short PAA homopolymers can undergo the transition to wormlike micelles. Once the PAA chains become too long, they must form ionic bonds with multiple PM2VP blocks. These PM2VP blocks are then bridged by a single PAA chain. To allow an increase in separation of the PM2VP blocks, and to follow the new contour of the worm-like micelle, the PAA chain must stretch, which is accompanied by a decrease in its configurational entropy. This entropic penalty apparently prevents the transition from spherical to wormlike micelles.

■ CONCLUSIONS

We have performed a comprehensive study of the stability and morphology of complex coacervate core micelles formed from PAA and PM2VP-*b*-PEO. At low salt concentration and under charge stoichiometric conditions, these C3Ms are spherical, independent of the chain and block lengths of the polymers. Below a critical PAA length, the hydrodynamic radius of the micelles is independent of the PAA length and increases with increasing PM2VP length, from 20 up to 42 nm, because of an increase in the micellar aggregation number. Above this critical PAA length, the hydrodynamic radius increases sharply with increasing PAA length because the C3M core can no longer accommodate a single PAA chain without a significant increase in size.

When salt is added, C3Ms start to disintegrate, and at a critical salt concentration, all micelles are disassembled. The critical salt concentration increases with increasing PAA and PM2VP length and levels off for long chains, in the same way as for macroscopic complex coacervates. Below the critical salt concentration, we find a nontrivial change in size of the various C3Ms: for long PAA chains, the micelles shrink upon addition of salt because of a decrease in the aggregation number, whereas for short PAA chains, they grow in size. A surprising morphological transition from spherical to wormlike micelles underlies this growth upon addition of salt. We rationalize the formation of wormlike micelles by an increase in the effective packing parameter, which does not occur for long PAA chains because of their interaction with multiple PM2VP blocks simultaneously.

■ ASSOCIATED CONTENT

Supporting Information

Light-scattering titration of $PM2VP_{41}$-*b*-PEO_{204} with PAA_{162}. Description of $c_{s,cr}$ determination from a light-scattering salt titration curve. Reversibility of the response of PAA_{1728}/$PM2VP_{41}$-*b*-PEO_{204} to salt. Description of N_{cr} determination from Figure 2a. Effect of salt on the cmc's of PAA_{13}/$PM2VP_{41}$-*b*-PEO_{204} and PAA_{139}/$PM2VP_{41}$-*b*-PEO_{204}. Estimation of the length of the wormlike micelles from D_r. Fitting parameters for the scattering curves in Figure 7. Critical scattering data on which Figure 8 is based. This material is available free of charge via the Internet at http://pubs.acs.org.

■ AUTHOR INFORMATION

Corresponding Author

*E-mail: hanne.vanderkooij@wur.nl; jasper.vandergucht@wur.nl.

Notes

The authors declare no competing financial interest.

■ ACKNOWLEDGMENTS

The small-angle X-ray experiments were performed at the European Synchrotron Radiation Facility (ESRF) in Grenoble at the ID02 high brilliance beamline. We are grateful for the beam time, and we kindly acknowledge technical support from our local contact T. Narayanan. E.S. acknowledges financial support from The Netherlands Organisation for Scientific Research (NWO). I.K.V. acknowledges financial support from The Netherlands Organisation for Scientific Research (VENI grant 700.10.406) and the European Union through the Marie Curie Fellowship (program FP7-PEOPLE-2011-CIG, contract no. 293788).

■ REFERENCES

(1) van der Gucht, J.; Spruijt, E.; Lemmers, M.; Cohen Stuart, M. A. Polyelectrolyte complexes: bulk phases and colloidal systems. *J. Colloid Interface Sci.* **2011**, *361*, 407−422.

(2) Lindhoud, S.; de Vries, R.; Norde, W.; Cohen Stuart, M. A. Structure and stability of complex coacervate core micelles with lysozyme. *Biomacromolecules* **2007**, *8*, 2219−2227.

(3) Kakizawa, Y.; Kataoka, K. Block copolymer micelles for delivery of gene and related compounds. *Adv. Drug Delivery Rev.* **2002**, *54*, 203−222.

(4) Oishi, M.; Nagasaki, Y.; Itaka, K.; Nishiyama, N.; Kataoka, K. Lactosylated poly(ethylene glycol)-siRNA conjugate through acid-labile β-thiopropionate linkage to construct pH-sensitive polyion complex micelles achieving enhanced gene silencing in hepatoma cells. *J. Am. Chem. Soc.* **2005**, *127*, 1624−1625.

(5) Lee, Y.; Ishii, T.; Kim, H. J.; Nishiyama, N.; Hayakawa, Y.; Itaka, K.; Kataoka, K. Efficient delivery of bioactive antibodies into the cytoplasm of living cells by charge-conversional polyion complex micelles. *Angew. Chem., Int. Ed.* **2010**, *49*, 2552−2555.

(6) Voets, I. K.; de Keizer, A.; Cohen Stuart, M. A. Complex coacervate core micelles. *Adv. Colloid Interfac.* **2009**, *147*, 300−318.

(7) Jang, W.-D.; Nakagishi, Y.; Nishiyama, N.; Kawauchi, S.; Morimoto, Y.; Kikuchi, M.; Kataoka, K. Polyion complex micelles for photodynamic therapy: incorporation of dendritic photosensitizer excitable at long wavelength relevant to improved tissue-penetrating property. *J. Controlled Release* **2006**, *113*, 73−79.

(8) Yan, Y.; Besseling, N. A. M.; de Keizer, A.; Marcelis, A.; Drechsler, M.; Cohen Stuart, M. A. Hierarchical self-assembly in solutions containing metal ions, ligand, and diblock copolymer. *Angew. Chem., Int. Ed.* **2007**, *46*, 1807−1809.

(9) Schwarz, S.; Dragan, S. Nonstoichiometric interpolyelectrolyte complexes as colloidal dispersions based on NaPAMPS and their interaction with colloidal silica particles. *Macromol. Symp.* **2004**, *210*, 185−192.

(10) van der Burgh, S.; Fokkink, R.; de Keizer, A.; Cohen Stuart, M. A. Complex coacervation core micelles as anti-fouling agents on silica and polystyrene surfaces. *Colloids Surf., A* **2004**, *242*, 167−174.

(11) Brzozowska, A.; Hofs, B.; de Keizer, A.; Fokkink, R.; Cohen Stuart, M.; Norde, W. Reduction of protein adsorption on silica and polystyrene surfaces due to coating with complex coacervate core micelles. *Colloids Surf., A* **2009**, *347*, 146−155.

(12) Kabanov, A. V.; Bronich, T. K.; Kabanov, V. A.; Yu, K.; Eisenberg, A. Soluble stoichiometric complexes from poly(*N*-ethyl-4-vinylpyridinium) cations and poly(ethylene oxide)-*block*-polymethacrylate anions. *Macromolecules* **1996**, *29*, 6797−6802.

(13) Yan, Y.; de Keizer, A.; Cohen Stuart, M. A.; Drechsler, M.; Besseling, N. A. M. Stability of complex coacervate core micelles containing metal coordination polymer. *J. Phys. Chem. B* **2008**, *112*, 10908−10914.

(14) Wang, J.; de Keizer, A.; Fokkink, R.; Yan, Y.; Cohen Stuart, M. A.; van der Gucht, J. Complex coacervate core micelles from iron-based coordination polymers. *J. Phys. Chem. B* **2010**, *114*, 8313−8319.

(15) Gaucher, G.; Dufresne, M.-H.; Sant, V. P.; Kang, N.; Maysinger, D.; Leroux, J.-C. Block copolymer micelles: preparation, characterization and application in drug delivery. *J. Controlled Release* **2005**, *109*, 169−188.

(16) Harada, A.; Kataoka, K. Formation of stable and monodispersive polyion complex micelles in aqueous medium from poly(L-lysine) and poly(ethylene glycol)-poly(aspartic acid) block copolymer. *J. Macromol. Sci. A* **1997**, *34*, 2119−2133.

(17) Dautzenberg, H.; Rother, G. Response of polyelectrolyte complexes to subsequent addition of sodium chloride: time-dependent static light scattering studies. *Macromol. Chem. Phys.* **2004**, *205*, 114−121.

(18) Matralis, A.; Sotiropoulou, M.; Bokias, G.; Staikos, G. Water-soluble stoichiometric polyelectrolyte complexes based on cationic comb-type copolymers. *Macromol. Chem. Phys.* **2006**, *207*, 1018−1025.

(19) Park, J.-S.; Akiyama, Y.; Yamasaki, Y.; Kataoka, K. Preparation and characterization of polyion complex micelles with a novel thermosensitive poly(2-isopropyl-2-oxazoline) shell via the complexation of oppositely charged block ionomers. *Langmuir* **2007**, *23*, 138−146.

(20) Pispas, S. Complexes of polyelectrolyte-neutral double hydrophilic block copolymers with oppositely charged surfactant and polyelectrolyte. *J. Phys. Chem. B* **2007**, *111*, 8351−8359.

(21) Lindhoud, S.; Voorhaar, L.; de Vries, R.; Schweins, R.; Cohen Stuart, M. A.; Norde, W. Salt-induced disintegration of lysozyme-containing polyelectrolyte complex micelles. *Langmuir* **2009**, *25*, 11425−11430.

(22) Soliman, G. M. *Polysaccharide-Based Polyion Complex Micelles as New Delivery Systems for Hydrophilic Cationic Drugs*. Ph.D. thesis, Faculty of Pharmacy, University of Montreal, 2009.

(23) Brzozowska, A.; Zhang, Q.; de Keizer, A.; Norde, W.; Cohen Stuart, M. Reduction of protein adsorption on silica and polysulfone surfaces coated with complex coacervate core micelles with poly(vinyl alcohol) as a neutral brush forming block. *Colloids Surf., A* **2010**, *368*, 96−104.

(24) Brzozowska, A.; de Keizer, A.; Christophe, D.; Cohen Stuart, M. A.; Norde, W. Grafted ionomer complexes and their effect on protein adsorption on silica and polysulfone surfaces. *Colloid Polym. Sci.* **2010**, *288*, 1621−1632.

(25) van der Burgh, S.; de Keizer, A.; Cohen Stuart, M. A. Complex coacervation core micelles. Colloidal stability and aggregation mechanism. *Langmuir* **2004**, *20*, 1073−1084.

(26) Ma, R.; Wang, B.; Liu, X.; An, Y.; Li, Y.; He, Z.; Shi, L. Pyranine-induced micellization of poly(ethylene glycol)-block-poly(4-vinylpyridine) and pH-triggered release of pyranine from the complex micelles. *Langmuir* **2007**, *23*, 7498−7504.

(27) Lemmers, M.; Voets, I. K.; Cohen Stuart, M. A.; van der Gucht, J. Transient network topology of interconnected polyelectrolyte complex micelles. *Soft Matter* **2011**, *7*, 1378−1389.

(28) Cohen Stuart, M. A.; Besseling, N. A. M.; Fokkink, R. G. Formation of micelles with complex coacervate cores. *Langmuir* **1998**, *14*, 6846−6849.

(29) Danial, M.; Klok, H.-A.; Norde, W.; Cohen Stuart, M. A. Complex coacervate core micelles with a lysozyme-modified corona. *Langmuir* **2007**, *23*, 8003−8009.

(30) Lindhoud, S.; de Vries, R.; Schweins, R.; Cohen Stuart, M. A.; Norde, W. Salt-induced release of lipase from polyelectrolyte complex micelles. *Soft Matter* **2009**, *5*, 242−250.

(31) Overbeek, J. T. G.; Voorn, M. J. Phase separation in polyelectrolyte solutions. Theory of complex coacervation. *J. Cell. Comp. Physiol.* **1957**, *49*, 7−26.

(32) Hunt, J. N.; Feldman, K. E.; Lynd, N. A.; Deek, J.; Campos, L. M.; Spruell, J. M.; Hernandez, B. M.; Kramer, E. J.; Hawker, C. J. Tunable, high modulus hydrogels driven by ionic coacervation. *Adv. Mater.* **2011**, *23*, 2327−2331.

(33) Capito, R. M.; Azevedo, H. S.; Velichko, Y. S.; Mata, A.; Stupp, S. I. Self-assembly of large and small molecules into hierarchically ordered sacs and membranes. *Science* **2008**, *319*, 1812−1816.
(34) Wu, H. Correlations between the Rayleigh ratio and the wavelength for toluene and benzene. *Chem. Phys.* **2010**, *367*, 44−47.
(35) Lide, D., Ed. *CRC Handbook of Chemistry and Physics*, 82nd ed.; CRC Press: Boca Raton, FL, 2001−2002.
(36) Harada, A.; Kataoka, K. Effect of charged segment length on physicochemical properties of core-shell type polyion complex micelles from block ionomers. *Macromolecules* **2003**, *36*, 4995−5001.
(37) Brandrup, J.; Immergut, E. H. *Polymer Handbook*, 3rd ed.; John Wiley & Sons: New York, 1989.
(38) Schillén, K.; Brown, W.; Johnsen, R. M. Micellar sphere-to-rod transition in an aqueous triblock copolymer system. A dynamic light scattering study of translational and rotational diffusion. *Macromolecules* **1994**, *27*, 4825−4832.
(39) Khlebtsov, B. N.; Khanadeev, V. A.; Khlebtsov, N. G. Observation of extra-high depolarized light scattering spectra from gold nanorods. *J. Phys. Chem. C* **2008**, *112*, 12760−12768.
(40) Spruijt, E.; Westphal, A. H.; Borst, J. W.; Cohen Stuart, M. A.; van der Gucht, J. Binodal compositions of polyelectrolyte complexes. *Macromolecules* **2010**, *43*, 6476−6484.
(41) Borisov, O. V.; Zhulina, E. B. Effect of salt on self-assembly in charged block copolymer micelles. *Macromolecules* **2002**, *35*, 4472−4480.
(42) Zhulina, E. B.; Adam, M.; LaRue, I.; Sheiko, S. S.; Rubinstein, M. Diblock copolymer micelles in a dilute solution. *Macromolecules* **2005**, *38*, 5330−5351.
(43) Voets, I. K.; de Vries, R.; Fokkink, R.; Sprakel, J.; May, R.; de Keizer, A.; Cohen Stuart, M. A. Towards a structural characterization of charge-driven polymer micelles. *Eur. Phys. J. E* **2009**, *30*, 351−359.
(44) Zhao, J. J.; Bae, S. C.; Xie, F.; Granick, S. Diffusion of polymer-coated nanoparticles studied by fluorescence correlation spectroscopy. *Macromolecules* **2001**, *34*, 3123−3126.
(45) Won, Y.-Y.; Davis, H. T.; Bates, F. S. Molecular exchange in PEO-PB micelles in water. *Macromolecules* **2003**, *36*, 953−955.
(46) Guragain, S.; Bastakoti, B. P.; Hasegawa, M.; Nakashima, K. Complex micelle formation between poly(ethylene oxide-b-N-methyl-2-vinylpyridinium iodide) and poly(methacrylic acid) in aqueous solutions. *Colloids Surf., A* **2010**, *363*, 86−91.
(47) Voets, I. K.; de Keizer, A.; Cohen Stuart, M. A.; Justynska, J.; Schlaad, H. Irreversible structural transitions in mixed micelles of oppositely charged diblock copolymers in aqueous solution. *Macromolecules* **2007**, *40*, 2158−2164.
(48) Voets, I. K.; Fokkink, R.; de Keizer, A.; May, R. P.; de Waard, P.; Cohen Stuart, M. A. On the transition between a heterogeneous and homogeneous corona in mixed polymeric micelles. *Langmuir* **2008**, *24*, 12221−12227.
(49) Spruijt, E.; Sprakel, J.; Cohen Stuart, M. A.; van der Gucht, J. Interfacial tension between a complex coacervate phase and its coexisting aqueous phase. *Soft Matter* **2010**, *6*, 172−178.
(50) Won, Y.-Y.; Bates, F. S. In *Giant Micelles: Properties and Applications*; Zana, R., Kaler, R., Eds.; CRC Press: New York, 2007; Chapter 14, pp 417−452.
(51) Aragon, S. R.; Flamik, D. High precision transport properties of cylinders by the boundary element method. *Macromolecules* **2009**, *42*, 6290−6299.
(52) Pecora, R. Laser light scattering and macromolecular Brownian motion. *Nature* **1971**, *231*, 73−75.
(53) Bastardo, L. A.; Garamus, V. M.; Bergström, M.; Claesson, P. M. The structures of complexes between polyethylene imine and sodium dodecyl sulfate in D_2O: a scattering study. *J. Phys. Chem. B* **2005**, *109*, 167−174.
(54) Voets, I. K.; van der Burgh, S.; Farago, B.; Fokkink, R.; Kovacevic, D.; Hellweg, T.; de Keizer, A.; Cohen Stuart, M. A. Electrostatically driven coassembly of a diblock copolymer and an oppositely charged homopolymer in aqueous solutions. *Macromolecules* **2007**, *40*, 8476−8482.
(55) Voets, I. K.; Leermakers, F. A. M. Self-consistent field theory for obligatory coassembly. *Phys. Rev. E* **2008**, *78*, 061801.
(56) Hayter, J. B.; Zulauf, M. Attractive interactions in critical scattering from non-ionic micelles. *Colloid Polym. Sci.* **1982**, *260*, 1023−1028.
(57) Liao, C.; Choi, S.-M.; Mallamace, F.; Chen, S.-H. SANS study of the structure and interaction of L64 triblock copolymer micellar solution in the critical region. *J. Appl. Crystallogr.* **2000**, *33*, 677−681.
(58) Schurtenberger, P.; Cavaco, C.; Tiberg, F.; Regev, O. Enormous concentration-induced growth of polymer-like micelles. *Langmuir* **1996**, *12*, 2894−2899.
(59) Israelachvili, J. N.; Mitchell, D. J.; Ninham, B. W. Theory of self-assembly of hydrocarbon amphiphiles into micelles and bilayers. *J. Chem. Soc., Faraday Trans. 2* **1976**, *72*, 1525−1568.
(60) Unsworth, L. D.; Sheardown, H.; Brash, J. L. Protein resistance of surfaces prepared by sorption of end-thiolated poly(ethylene glycol) to gold: effect of surface chain density. *Langmuir* **2005**, *21*, 1036−1041.